# *A Worldwide Theoretical Comparison of Outdoor Potential for Various Silicon-Based Tandem Module Architecture*

Cell Reports
Physical Science

CellPress

Article

# A Worldwide Theoretical Comparison of Outdoor Potential for Various Silicon-Based Tandem Module Architecture

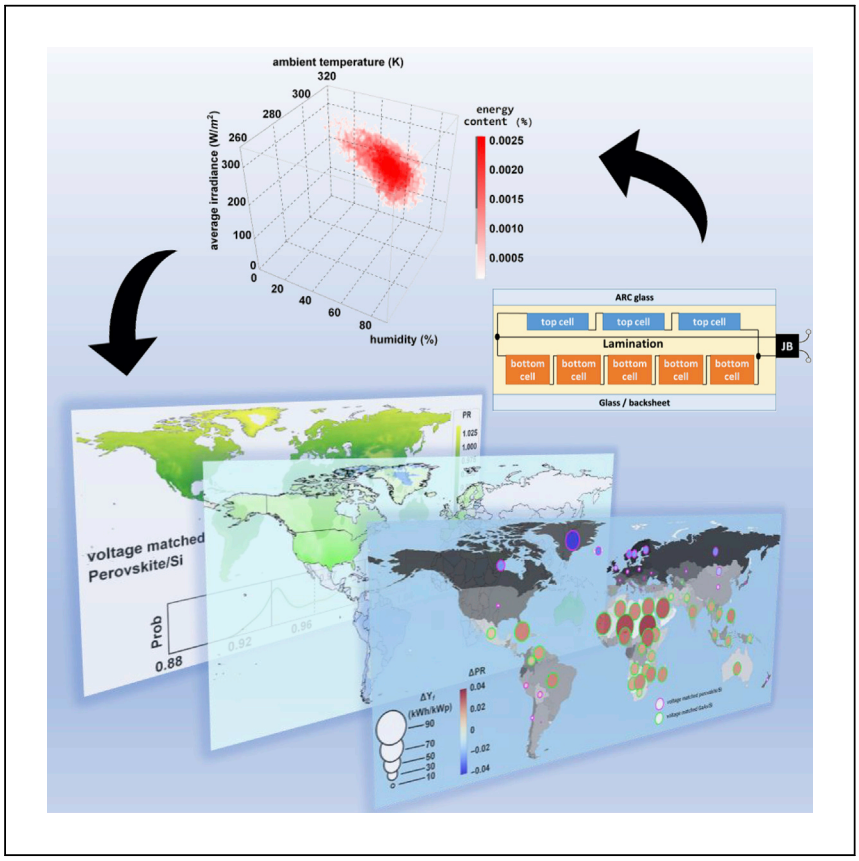


Tandem modules are the next step in the development of silicon-based tandem technology. Here, Liu et al. present an evaluation framework to compare outdoor performance potential for different tandem architectures globally, in different climate zones. In addition, techno-economic analysis offers a preliminary assessment of practical viability.

Haohui Liu, Carlos D. Rodríguez-Gallegos, Zhe Liu, Tonio Buonassisi, Thomas Reindl, Ian Marius Peters

liu.haohui@u.nus.edu

## HIGHLIGHTS

Side by side comprehensive comparison among tandem module architectures

Global energy yield and performance ratio calculation

Established relative advantages of different architectures in various climate zones

Derived boundary conditions for tandem modules to be economically successful

Liu et al., Cell Reports Physical Science 1, 100037
April 22, 2020 
https://doi.org/10.1016/j.xcrp.2020.100037

Cell Reports
Physical Science

CellPress

Article

# A Worldwide Theoretical Comparison of Outdoor Potential for Various Silicon-Based Tandem Module Architecture

Haohui Liu,[1,3,*] Carlos D. Rodríguez-Gallegos,[1] Zhe Liu,[2] Tonio Buonassisi,[2] Thomas Reindl,[1] and Ian Marius Peters[2]

## SUMMARY

**Silicon-based multi-junction (tandem) technology is one potential route to the next breakthrough for terrestrial photovoltaic conversion. Significant progress has been made in tandem solar cells. To move forward, development of tandem module technology is essential. Here, we theoretically compare five possible tandem module architectures with multiple material combinations by modeling their outdoor performance ratios around the globe. This framework aids in evaluating future module designs and technology pathways by relating lab-based efficiency to field performance and even project financing. We find that tandem performance ratios depend notably on climate conditions. In general, three-terminal and mechanically voltage-matched modules show exceptionally good outdoor performance. Furthermore, we investigate the implications of technical performance on manufacturing cost globally and find that tandems are promising in high-value markets in arid climates, where a three to five times increase in the current silicon module manufacturing cost is allowed under an optimistic scenario.**

## INTRODUCTION

Solar cells and photovoltaic (PV) applications have undergone phenomenal advances during the last decades. The efficiencies of some major solar cell technologies, such as silicon (Si) wafer and gallium arsenide (GaAs) solar cells, are already approaching their theoretical limits.[1–3] While the balance of system (BOS) and other system-related costs also continue to fall, the fastest way to reduce the levelized cost of energy (LCOE) of solar electricity is increasing the PV conversion efficiency beyond the current efficiency limits, which allows for better utilization of the BOS and eventually boosts the competitiveness of PV against traditional sources of energy.[4,5] Si-based multi-junction (tandem) technology (i.e., stacking one or more top cells of higher bandgaps onto Si) is one such pathway. This approach leverages the material abundance, technological maturity, and cost competitiveness of Si and couples it with top cells, such as GaAs, indium gallium phosphide (InGaP), and perovskite. Recently, rapid progress was made in Si-based tandem solar cells using mechanical stacking and wafer bonding. In laboratories, >32% efficiency has been demonstrated using III-V top cells on Si,[6,7] and 28% for a perovskite-on-Si (perovskite-Si) tandem.[1,8,9] These tandem efficiencies already surpassed the record for single-junction (SJ) Si solar cells (26.7%[3]), revealing their great potential.

One important feature of tandem technology is that there are multiple ways to integrate the top and bottom cells. Furthermore, the integration can be done beyond

[1]Solar Energy Research Institute of Singapore, National University of Singapore, Singapore

[2]Massachusetts Institute of Technology, Cambridge, MA, USA

[3]Lead Contact

*Correspondence: liu.haohui@u.nus.edu

https://doi.org/10.1016/j.xcrp.2020.100037

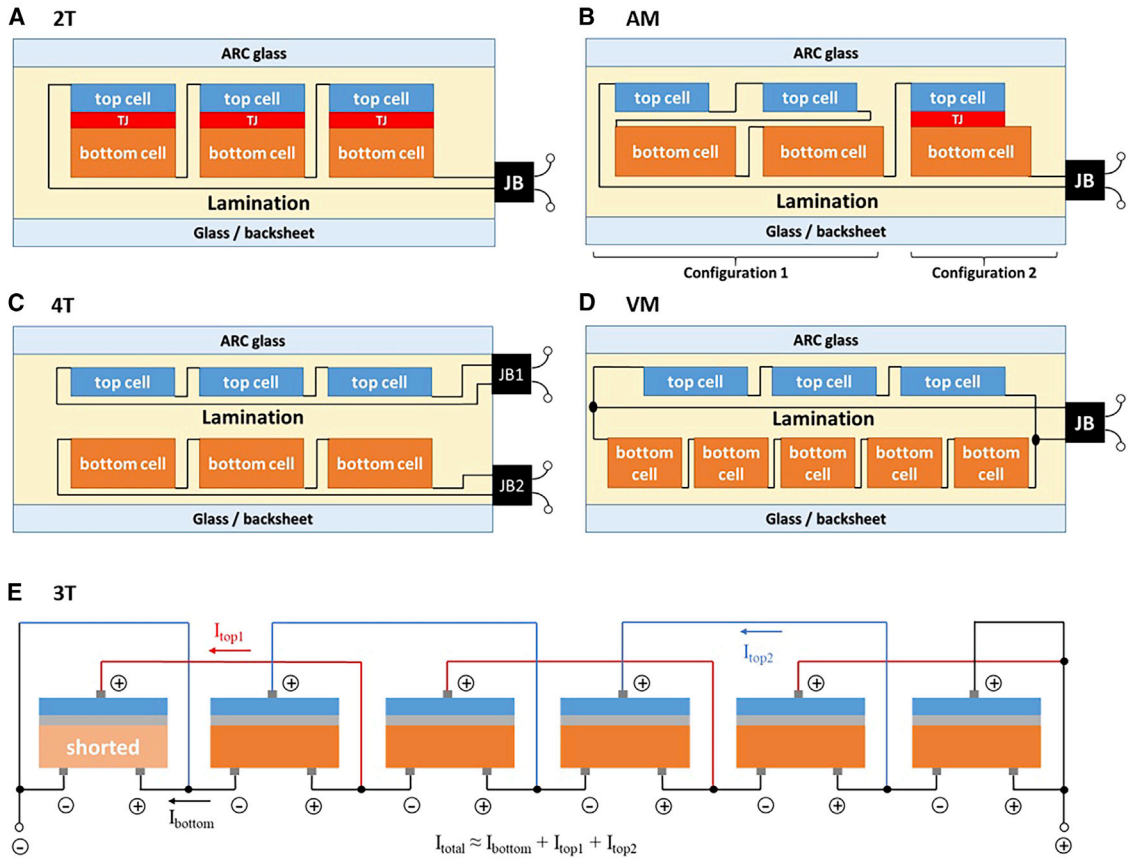


**Figure 1. Conceptual Tandem Module Configurations under Investigation**

(A–E) (A) Two-terminal (2T), (B) areal-matched (AM), (C) four-terminal (4T), (D) mechanically voltage-matched (VM), and (E) three-terminal (3T).[15,32] ARC, anti-reflective coating; JB, junction box, which is required to realize tandem module connection on the system level; TJ, tunnel junction layer in a monolithic tandem solar cell.

the cell level—on the module level. Overall, the following architectures are possible (Figure 1): two terminal (2T), areal matched (AM),[10] four terminal (4T), mechanically voltage matched (VM),[11–13] and three terminal (3T).[13–19] The design space of actual tandem modules is much broader, as they can assume various configurations, with different material systems, bandgap combination, cell structures, spatial layout, metallization schemes, fabrication methods, and many others. For cell and module manufacturers, it is important to be able to evaluate the different technology options, or pathways, as it affects their strategy and investments. Toward that goal, tandem configurations may be compared and assessed based on the following aspects:

1. Efficiency limit, which indicates the potential for a general tandem family under ideal assumptions. This has been investigated in numerous studies.[12,20–23]
2. Actual efficiency level attained under standard test conditions (STCs), after taking into account practical limitations.
3. Manufacturing cost in $\$/W_p$; several techno-economic studies have tried to address the cost.[4,5,24]
4. Outdoor performance, which gives the final energy yield.

Aspects 3 and 4, together with other system-related costs, determine the final LCOE of a project, which is usually the ultimate measure in large-scale applications. While many studies had explored the efficiency and cost of tandem solar cells, there is still

much uncertainty in these elements regarding actual tandem modules that may be realized in the future. Outdoor performance, however, may be more generalizable for a given architecture, as it depends primarily on the characteristic losses of that architecture under prevailing operating environments. It is known that different tandem architectures perform differently in outdoor environments, which can deviate substantially from STCs for which modules are designed and optimized.[25] Therefore, it is desirable to quantitatively assess the actual outdoor performance under different climatic conditions, instead of merely looking at their STC efficiencies. This is useful in answering the following questions:

What is the relative outdoor performance among different tandem architectures?
How important is it to consider climates when deploying tandem devices? Which tandem is most suitable under each climate?
How do tandems perform compared to SJ technologies? In which climate does it make the most sense to switch to tandems?
How much variation in performance is there across the globe? Is customization of design needed?
What are the implications of the technical performance on their economic viability?

Outdoor performance can be characterized by energy yield and implied performance ratio (PR), which is related to a common metric used in assessing system efficiency relative to the rated capacity under STCs (see Experimental Procedures). In real applications, device efficiency is not directly factored into the calculation, as one can always build the same capacity with different technologies. Instead, PR (and thus specific energy yield) and cost provide a more direct and convenient way than device efficiency to evaluate technology competitiveness for PV system applications. Several energy yield studies investigated field potential for tandem devices using outdoor conditions from specific locations,[26–33] but they are limited in the comprehensiveness of tandem configurations investigated or in the extensiveness of geographic coverage. In addition, they use different models and methodologies, which makes cross-comparison and evaluation challenging.

In this article, we evaluate the various tandem module architectures from the perspective of outdoor performance and the implied LCOE in different climates. We extend previous yield studies with a comprehensive geographical coverage, a more complete set of material systems, and more suitable device models to predict and compare tandem behavior side by side to provide a holistic view. Energy yield calculations are performed using satellite-derived meteorological data from the NASA as input.[34] The implied PR is then calculated to facilitate comparison among different architectures and across different climate zones to reach more generalizable conclusions. Device calculations are based on a two-diode model incorporating photon recycling and luminescent coupling (LC) effects[35] for Si and III-V sub-cells, or a physics-based analytical model[36] for perovskite sub-cells. In terms of efficiency, we assumed best theoretical modules derived from record-level devices as a case study to motivate future development while remaining somewhat realistic. However, this study should not be taken as a comparison of the absolute performance of specific tandem designs or optimization strategies; the use of PR as a metric for comparison is thus more generalizable as it reflects the characteristic losses of a given architecture, thereby reducing the bias caused by the different device properties and efficiencies assumed (see Note S1). We did not explicitly consider module manufacturing cost in $\$/W_p$, as there is still uncertainty regarding the actual path of realizing them, but we performed LCOE calculations to advise on the allowed

manufacturing cost increase compared to conventional Si technology under various scenarios (see Experimental Procedures). These results can help to shed light on the general outdoor characteristics of various tandem architectures to guide the evaluation of future designs of commercial tandem modules and their cost targets. For system designers and the broader industry, these results offer a preliminary assessment of the practical viability of flat-plate tandem technology in different parts of the world.

## RESULTS

### Tandem Module Architectures and Characteristics

The characteristics of the five theoretically possible tandem module architectures shown in Figure 1 are explained as follows:

In 2T, monolithic tandem cells (Figure 1A) are connected like a normal SJ cell into a module. This architecture has the greatest sensitivity toward variations in the solar spectrum due to current matching constraints.[25] On top of this, the current matching condition may change slightly with temperature, particularly for perovskite on Si, whose sub-cells have opposite bandgap dependence on temperature.[31]

AM modules allow for two configurations: one is to connect a group of series-connected top cells with a group of series-connected bottom cells, called "configuration 1" in Figure 1B; another is similar to the 2T configuration, with monolithic tandem cells connected in series ("configuration 2"). In both cases, the areas of top and bottom cells are adjusted to produce the same current.

For 4T modules (Figure 1C), the top and bottom cells can be connected in such a way that a module has two junction boxes or has a power optimizer to independently track the maximum power point (MPP) of the top and bottom cells. In the first case, all of the top and bottom junction boxes can be connected and then fed to different inverters separately, constituting two independent strings. In this way, there is no need for additional power electronics to properly aggregate power produced from the top and bottom cells. The dependence of 4T toward operating conditions is a combined effect of the dependence of its sub-cells.

For VM modules (Figure 1D), a string of series-connected top cells is connected in parallel with another string of series-connected bottom cells in a mechanically stacked fashion. Voltage is matched by adjusting the number of cells in each string. Similar to 4T, the mechanical stacking may circumvent various constraints associated with the conventional monolithic integration on the cell level. Voltage matching shows much less sensitivity toward spectral variations, as there is no requirement for current matching. However, it is expected to show some sensitivity toward temperature changes when there is a mismatch between temperature coefficients ($T_C$) and bandgap dependence of the top and bottom cells.[16]

Alternatively, voltage matching can also be achieved with monolithically integrated tandem cells with 3T,[13–19] which is a promising architecture that has recently attracted increasing amounts of interest. 3T tandem has the advantage of being monolithic, which avoids additional layers and thus parasitic optical absorption losses during module integration, while still allowing flexibility in bandgap combinations. 3T cell or module behavior is more complicated but in principle closely resembles that of a mechanically stacked VM module.[13]

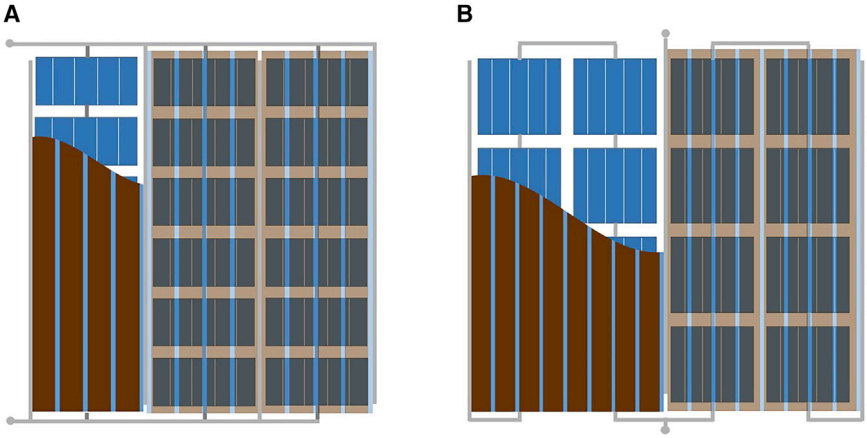


**Figure 2. Possible Layout of Tandem Modules**

(A) An example of VM module layout with three groups of parallel connected half-cut Si bottom cells (blue) and thin-film top cells (brown). Stripes of thin-film top cells are connected by transparent conductive oxides (light blue).

(B) An example of AM module layout with two groups of series-connected top and bottom cells. Module metallization (ribbons) are shown in gray.

Future full-scale tandem module designs will very likely follow one of these architectures. In this work, the architectures are treated in an abstract and conceptual way, without constraining the actual way of realization. As an illustration, a possible realization of AM and VM in an actual module is depicted in Figure 2. Although the integration schemes may not be practical now, it is still desirable to include them in the comparison, as the technical obstacles may be resolved in the future.

For simplicity, during simulation we model the smallest repeatable pair of sub-cells or group of top and bottom cells as a unit tandem module. The configurations investigated in the present study for each architecture are listed in Table 1, together with their simulated STC efficiencies and $T_C$ at the MPP. The optical absorption in the sub-cells is calculated using measured sub-cell external quantum efficiency (EQE) of record tandem solar cells from the literature. These EQEs reflect the representative optical structure of a tandem architecture; therefore, no optical model is invoked to further calculate the currents. The electrical properties of high-quality, record-level sub-cells are assumed for each tandem configuration. Details about the electrical parameters and other modeling assumptions are presented in Tables S1–S3.

As an example, Figure 3 shows the modeled perovskite-Si tandem efficiency with respect to spectral composition (characterized by average photon energy of the spectra set found in Singapore,[42] calculated for the wavelength range 350–1,060 nm), intensity level, and temperature. A few observations can be made. 3T, 4T, and VM perovskite-Si efficiencies change only mildly with spectrum, while 2T and AM efficiencies show large dependence, as expected. However, this may change slightly when strong LC is present.[43] AM behaves very similarly to 2T, except that it shows slightly less sensitivity toward spectral changes. VM exhibits a more pronounced efficiency drop toward low intensities. In contrast, 3T has exceptional low-light performance because in this case, the perovskite string is voltage limiting, so the tandem low-light behavior is dominated by that of perovskite, which is less sensitive to irradiance levels. We also note that the temperature dependence of tandems tends to be more complicated than SJ modules due to the shifting weights of

**Table 1. Configurations Investigated in This Work for Each Architecture**

| Configuration (Tandem or SJ) | STC Efficiency (%) | References for EQE | $T_C$ (Relative-%/K)[a] |
|---|---|---|---|
| 2T GaAs-Si | 29.2 | Liu et al., 2017[37,b] | 0.20 |
| 3T GaAs-Si | 33.0 | Essig et al., 2017[6] | 0.14 |
| 4T GaAs-Si | 34.2 | Essig et al., 2017[6] | 0.17 |
| AM GaAs-Si | 31.3 | Essig et al., 2017[6] | 0.20 |
| VM GaAs-Si | 33.9 | Essig et al., 2017[6] | 0.15 |
| 2T InGaP-Si | 28.3 | Liu et al., 2017[37] | 0.13 |
| 3T InGaP-Si | 34.5 | Essig et al., 2017[6] | 0.20 |
| 4T InGaP-Si | 34.7 | Essig et al., 2017[6] | 0.17 |
| VM InGaP-Si | 34.7 | Essig et al., 2017[6] | 0.16 |
| 2T InGaP/GaAs-Si | 33.2 | Essig et al., 2017[6] | 0.15 |
| 2T perovskite-Si | 30.8 | Sahli et al., 2018[9] | 0.25 |
| 3T perovskite-Si | 25.6 | Werner et al., 2016[38] | 0.20 |
| 4T perovskite-Si | 27.5 | Werner et al., 2016[38] | 0.24 |
| AM perovskite-Si | 27.3 | Werner et al., 2016[38] | 0.23 |
| VM perovskite-Si | 27.4 | Werner et al., 2016[38] | 0.26 |
| Si (HJT) | 26.2 | Yoshikawa et al., 2017[3] | 0.26 |
| Si (PERC) | 21.3 | Fell et al., 2014[39] | 0.36 |
| GaAs | 28.1 | Kayes et al., 2011[2] | 0.14 |
| Perovskite | 21.7 | Yang et al., 2017[40] | 0.22 |
| InGaP | 19.7 | Geisz et al., 2013[41] | 0.10 |

Calculated efficiency and MPP TC under STC for the various tandem and SJ configurations under investigation. Tandem efficiencies are calculated assuming optics of record tandem EQEs but electrical properties of record SJ cells. Optical structure of 4T is assumed for 3T, VM, and AM tandems. For InGaP-Si, the InGaP bandgap is too high to achieve current matching with Si, so 2T efficiency is lower than ideal. Note that 2T perovskite-Si assumes a different optical structure than the other architectures and therefore has a higher efficiency than the other perovskite tandems. All 3T tandems have a top to bottom ratio of 1:2 (one top cells in parallel with two bottom cells). AM, areal matched; EQE, external quantum efficiency; MPP, maximum power point; PERC, passivated emitter and rear cell; HJT, heterojunction technology; SJ, single junction; STC, standard test condition; 2T, two terminal; 3T, three terminal; 4T, four terminal; $T_C$, temperature coefficient; VM, voltage matched.

[a]Calculated under AM1.5G spectrum at one sun using device models outlined in Experimental Procedures.

[b]Optical absorption simulated using methodology presented in the literature.

influence from top and bottom sub-cells. The modeled efficiencies of SJ and other tandem configurations are presented in Figures S2 and S3.

## Outdoor Field Performance

In Figure 4, we show the predicted worldwide PR for tandem modules with perovskite and GaAs top cells in 2T and 4T architecture. In general, the highest PR is achieved in cold and high-altitude regions, where the temperature is lower. 2T shows much larger variation across the globe, with an interquartile range of PR ~0.08–0.1. Its PR suffers significantly in most parts of the tropical regions, largely due to significantly more blue-rich spectra resulting from low air mass and high water content.[26,42] In these regions, customization of design may be needed. In contrast, 4T shows reduced sensitivity to these differences and exhibits a more uniform PR across the globe (variation only ~0.04). In Figures S5–S8 and Notes S2 and S3, we also show the PR map of the other

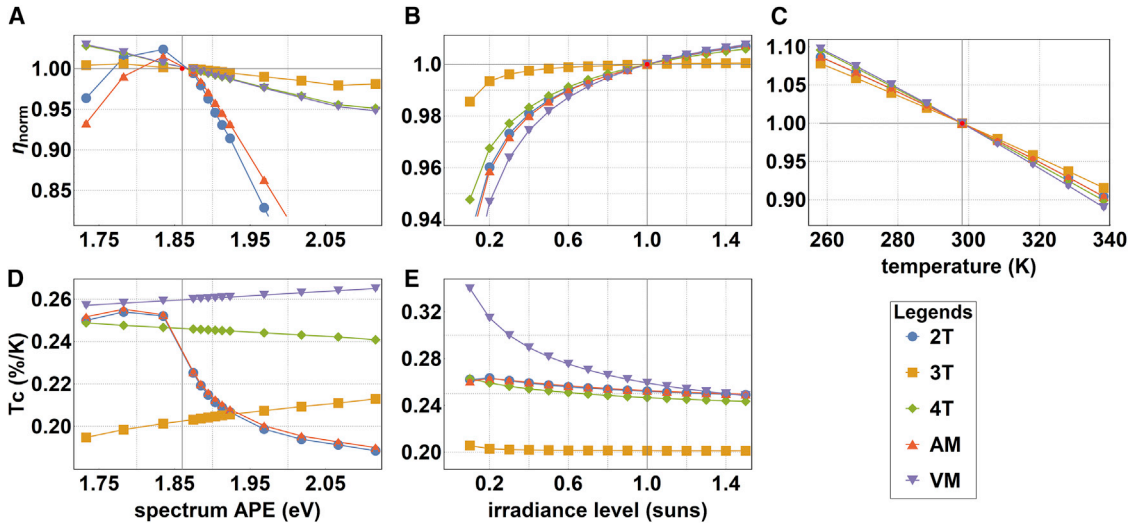


**Figure 3. Tandem Efficiencies and Temperature Coefficients under Varying Conditions**

(A–E) Efficiency of 2T, 3T, 4T, AM, and VM perovskite on Si tandems under (A) different spectra, (B) irradiance levels, and (C) temperature, normalized to their respective STC efficiencies (first row). Temperature coefficient at the MPP under (D) different spectra and (E) irradiance levels is shown in the second row. Vertical gray lines indicate STC.

architectures and SJ modules, as well as the difference between SJ and tandem. Assuming that the current record GaAs-Si represents the efficiency level attainable by mature tandem technologies, the 4T architecture generates on average ~20% (70 kWh/m$^2$) more yield than the 2T architecture and 60% (160 kWh/m$^2$) more yield than conventional passivated emitter and rear cell (PERC) Si modules, which are becoming the norm. For the current record level 2T perovskite-Si solar cell, the increase from Si SJ technology is 40% (112 kWh/m$^2$). This number is expected to increase as perovskite solar cell performance improves.[12]

## Performance in Different Climate Zones

To further understand the calculated worldwide field performance results, we grouped and analyzed tandem PR in four major climate zones (see climate zone classification map in Figure S4). We analyzed the operating conditions in each climate zone using NASA satellite data. The main parameters studied are irradiance level, temperature, humidity (which together with temperature determines the water vapor content in the atmosphere), and air mass (which influences the spectral distribution of sunlight). Figure 5 shows the energy content distribution with respect to daily average values of the irradiance, temperature, and humidity in each climate zone, which is color-coded. Air mass is primarily determined by latitude and is simply the same as the latitude distribution of the climate zones.

In general, temperate and cold climates have flatter distribution due to the strong presence of the seasons. Thus, the operating conditions span a wider range. In comparison, tropical and arid climates show prominent peaks in which most of the available insolation is contained. Arid zones have the highest temperatures and insolation and the lowest humidity. Tropical zones are mostly hot and humid, with mid- to high insolation, and show the least spread. As a result of the different distribution of operating conditions, tandem architectures are expected to show different PR drops in each climate zone. For instances, PR is usually highest in cold climates, as temperature loss is smaller. Low irradiance

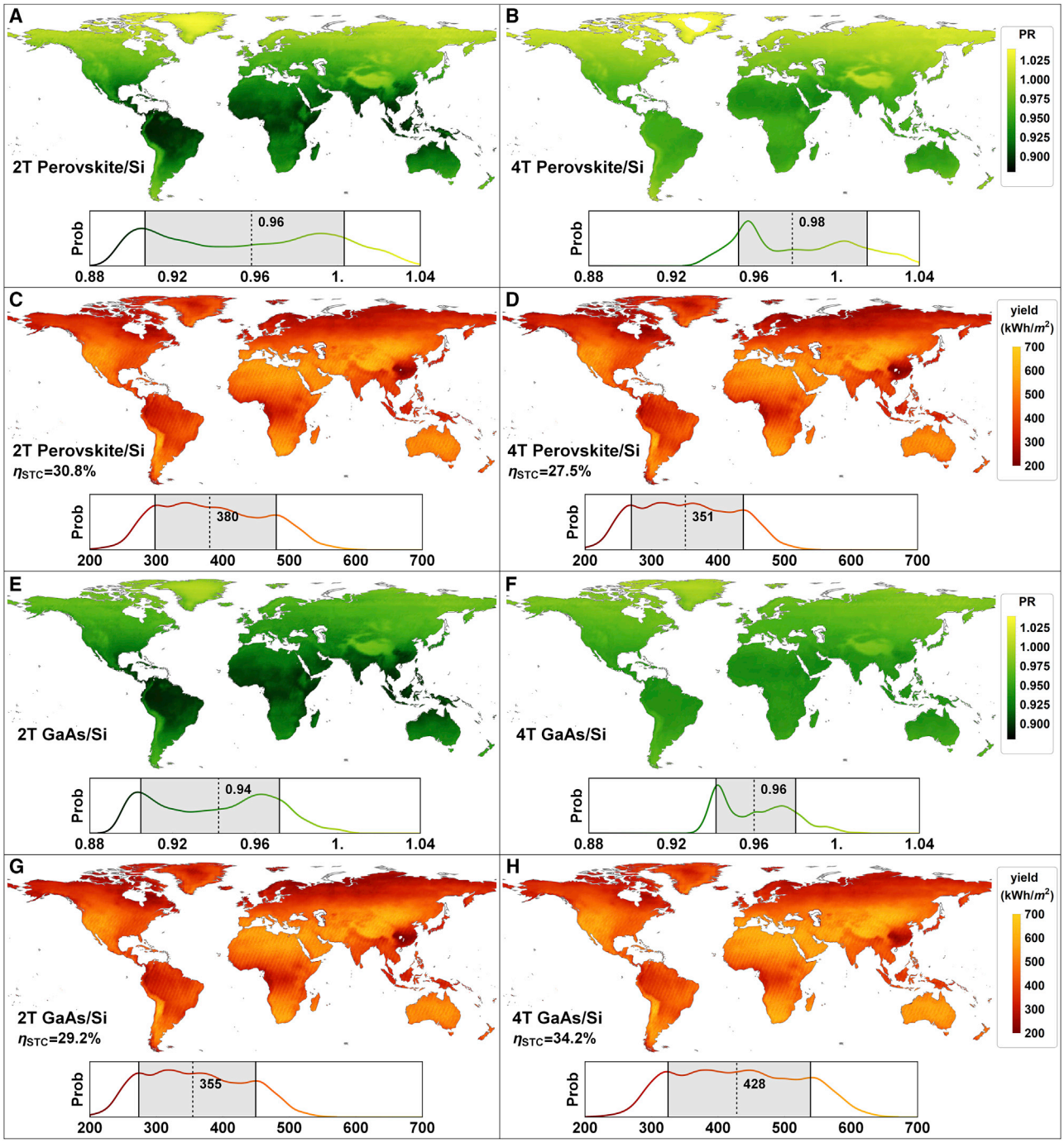


**Figure 4. Calculated Worldwide Implied Performance Ratio (PR)**

(A–H) PR for 2T and 4T perovskite-Si (A and B), GaAs-Si (E and F), as well as energy yields for 2T and 4T perovskite-Si (C and D) and GaAs-Si (G and H) for 2015. The distribution of values across the globe in terms of frequency of occurrence is shown in the smooth histogram beneath each plot, with the same color-coding as in the map. Also shown are the median values and the range between the upper and lower 15$^{th}$ percentile (highlighted gray). Geographic plots are produced by Mathematica 12.

loss is lowest in arid climates, as irradiance is generally higher. 2T tandems are expected to suffer from more blue-rich spectra in the tropics.[27,42] However, the exact overall effect combining these factors can only be determined from detailed calculations.

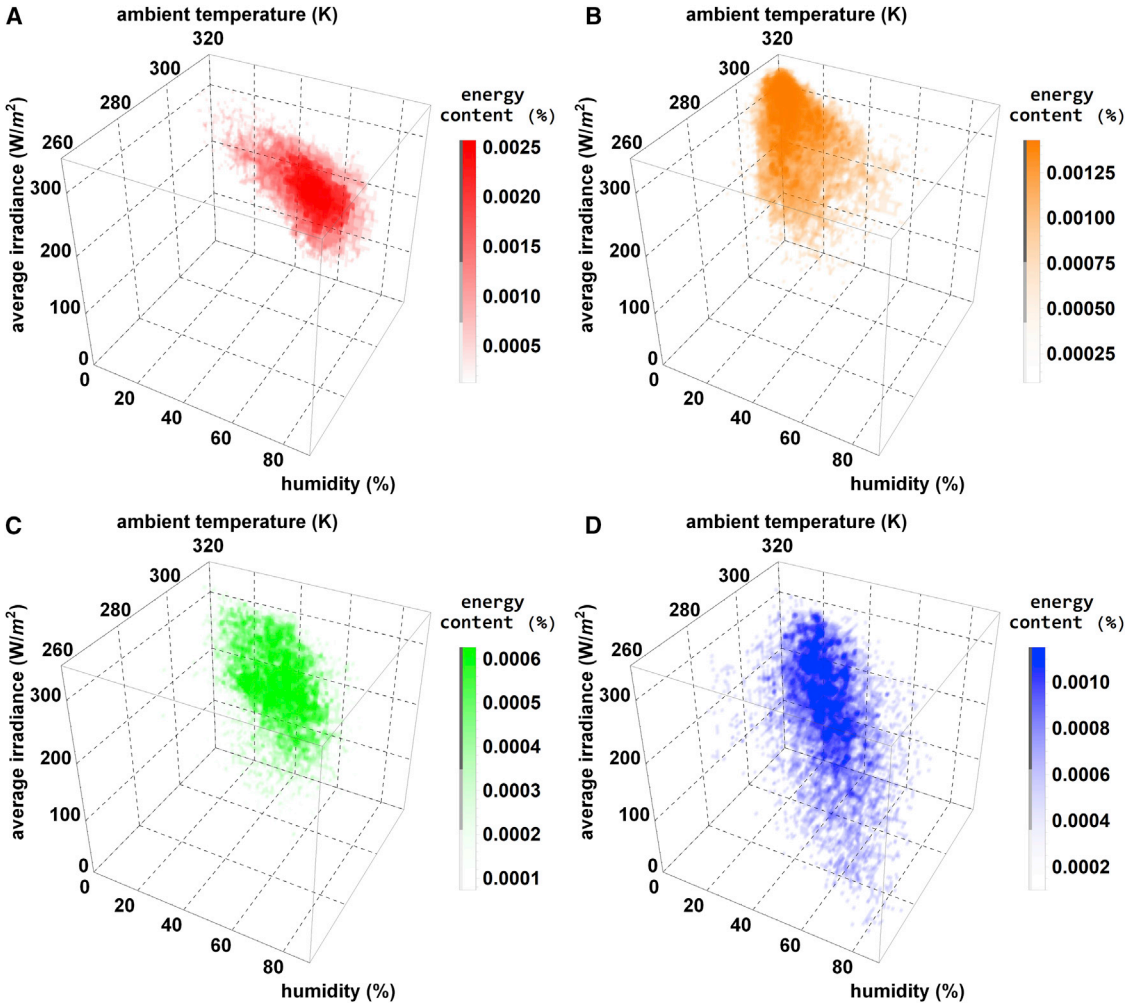


**Figure 5. 3D Density Plot of Energy Content Distribution**

(A–D) Energy content with respect to daily average values of the irradiance, temperature, and humidity in (A) tropical, (B) arid, (C) temperate, and (D) cold climates. The clusters shown represent the most relevant conditions that contain 75% of the total available insolation in an average location of the respective climate zones. Color saturation and transparency denote the amount of energy content (in percentage of total yearly total) within a bin of 10 $W/m^2$ (irradiance) × 1 K (temperature) × 2% relative humidity.

Figure 6 shows the area-weighted distribution of PR. Comparing across tandem architectures, a few observations can be made. In general, 4T tandems have the highest PR, as expected. The PR of VM tandems is quite close to that of 4T in all climate zones, with an absolute difference of only $\leq$0.015 on average for perovskite-Si, and even a slight gain for GaAs-Si. This is possible because the voltage is not exactly matched at the MPP under STCs. Therefore, when conditions change, the matching may improve from STCs. Overall, it turns out that the voltage mismatch loss created by elevated temperatures is not significant for the investigated material systems. Therefore, with the same installed capacity, VM tandem module can deliver energy yield over 98% of what is achievable by 4T. This may be further improved by module-level power electronics.[11] 3T tandems perform equally well or even better. In particular, 3T perovskite-Si has a much higher PR than 4T, mainly due to substantially imbalanced voltage matching under STCs. This improvement over 4T is also seen in a study by Schmager et al.[33] In this case, if the system can be realized with equal capacity and capital expenditure (capex), then 3T modules are actually

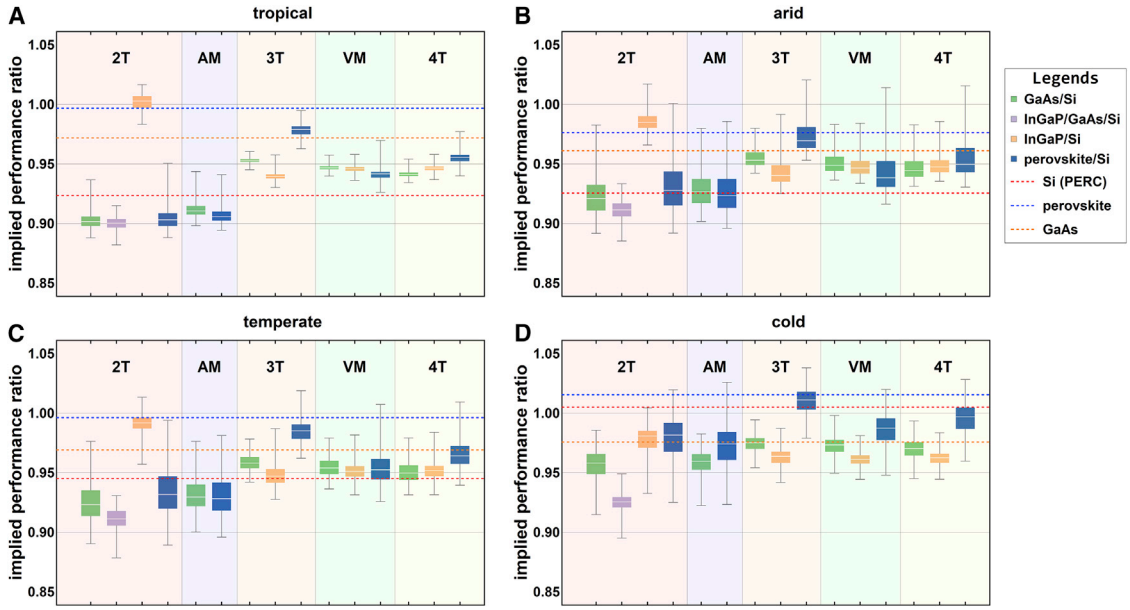


**Figure 6. Distribution of Calculated PR for Various Tandem Modules in Each Climate Zone in Box Whisker Plot**

(A–D) The grouped PR values contain sampled PRs calculated across the year in geographic grid points (in 1° × 1° resolution) from a given climate zone: tropical (A), arid (B), temperate (C), and cold (D). The sampling is area weighted so that high-latitude regions are not overrepresented. The average PR for single-junction (SJ) modules in each climate zone is also indicated in the figure as dashed lines. Boxes represent 25$^{th}$–75$^{th}$ quantiles; whiskers and fences (error bars) represent the range from minimum to maximum.

preferred over 4T, despite the fact that they have non-ideal matching under STCs and have lower STC efficiency. However, the simplified perovskite models used here do not account for the parasitic shunt resistance that will likely be present in scaled-up perovskite top cells, resistive losses in Si bottom cells, and the partially shorted cell at the end of each string. The inclusion of these effects will no doubt lead to a lower PR, which may make it similar to that of 3T GaAs-Si. Overall, these results corroborate those from previous calculations for 3T tandem solar cells and VM modules for several locations in the United States.[11,28,32,33] III-V and perovskite materials could be made into different bandgaps. These variations may produce slightly different PR for the various architectures. However, investigation of the full space of the design is beyond the scope of the present work.

2T and AM tandems are of a similar type, which are both current matched. It is not surprising that they have very similar PRs, and as a group, their PR is noticeably lower than that of 4T tandems (due to sensitivity to spectral variation) and is nearly always lower than that of SJ modules, with the only exception being 2T InGaP-Si, whose high PR is primarily due to improvement from imperfect STC current matching in the field (similar to the case of 3T perovskite-Si). Other than the PR in cold climates, their PR is generally lower than 4T by 0.02–0.05. Nonetheless, in temperate and arid climates, all double-junction tandems can reach similar (>97%) PR levels as SJ Si, which is in agreement with findings from the literature for specific locations.[28,30] In contrast, triple-junction 2T tandems achieve the highest-rated (STC) efficiency, but tend to have lower PR than double-junction tandems in all climate zones; therefore, not all STC efficiency benefits can be retained in the field. Readers may refer to Table S5 for a comparison of final harvesting efficiencies and energy yields. Our calculation only considers monofacial modules. In bifacial applications, the advantages of 3T, 4T, and VM arguably would be even larger. Modeling bifacial gain would require

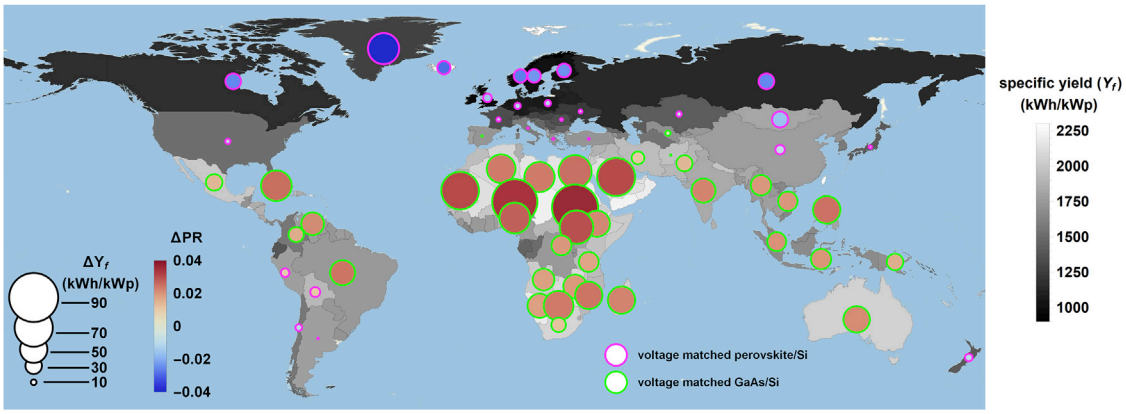


**Figure 7. Outdoor Performance Comparison between VM GaAs-Si or Perovskite-Si (Whichever is Higher) and SJ PERC Si across Countries**

Grayscale background shows the average energy yield per $kW_p$ of installed PV ($Y_f$) of VM tandem in each country. The bubble radius and fill color indicate the difference in the specific yield and PR, respectively. The bubble edge color denotes which material combination provides the higher performance.

an additional calculation module for determining rear irradiance from a more detailed sky model and a modified optical model to account for rear absorption. These can be incorporated into our modeling framework as future work.

## VM Tandems

Through this work, we find that the tandem architectures with voltage matching (i.e., 3T and VM) are promising candidates for field application. They have exceptionally good outdoor performance with high PR and smaller variation across different climate zones. At the same time, they can relax the constraints of material bandgaps, and have only two terminals, which do not require more complicated circuits to connect modules on the system level, as in the case of 4T.

Figure 7 shows in detail the outdoor performance potential of VM tandems compared to SJ PERC Si. To simplify the graphic representation, we depict average values per country. We have calculated performance using two material systems: GaAs-Si and perovskite-Si. In each country, the results from the material combination that gives the higher PR is presented: the green bubble edge indicates an advantage for GaAs-Si and purple for perovskite-Si. The background in grayscale shows the specific final yield ($Y_f$) achieved by the VM tandem in a typical meteorological year. The bubble radius and fill color indicate the difference in $Y_f$ and PR, respectively, compared to SJ Si. Brown bubbles mean that the tandem has a higher PR and thus higher specific yield than SJ Si, whereas blue bubbles mean the opposite. One conspicuous observation is that the VM tandem performs much better than Si in the vast majority of Africa, South Asia and Southeast Asia, the Middle East, Central and South America, and arid regions in Australia, which are mostly hot and sunny regions. However, it performs worse than Si in temperate and cold climates because Si has a higher $T_C$. However, as the available solar resource in these places is also smaller, the difference in the $Y_f$ is greatly reduced (blue but smaller bubbles). It would appear that conditions that favor tandems also have higher insolation. This synergistic effect should improve the competitiveness of tandems in these regions. Incidentally, in all of the regions in which tandem PR is greater than SJ PR, GaAs-Si outperforms perovskite-Si and vice versa in this simulated case.

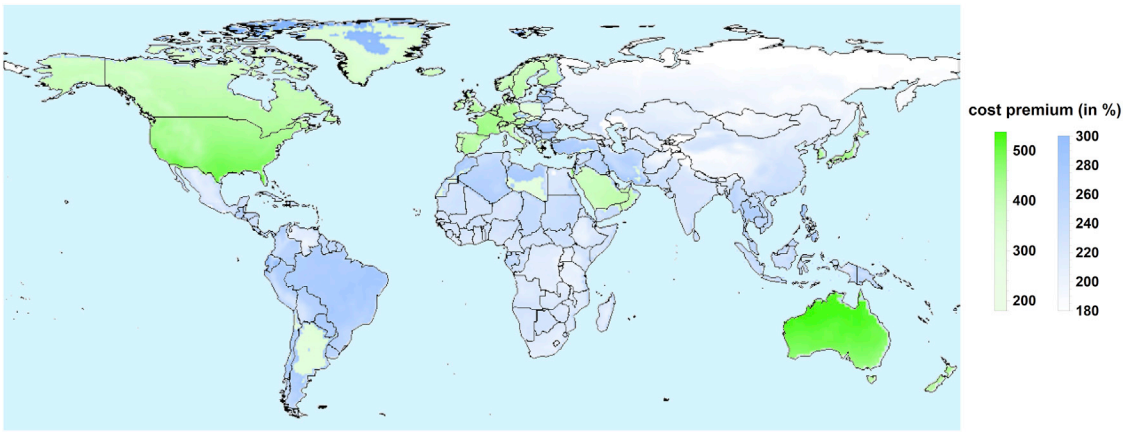


**Figure 8. Calculated Worldwide Cost Premium**

The allowed cost premium in module fabrication cost for 4T GaAs-Si tandem as compared to PERC Si, assuming residential cost scenario worldwide. The magnitude of the cost premium of 4T tandem in percentage of Si module cost is represented by saturation. The added dimension of color serves to indicate the situation of other tandem architectures. The green color indicates that cost premium of all tandem architectures surpasses 180%; the blue color indicates that only cost premium of 4T and VM tandem does.

## Cost Considerations

High efficiency level and outdoor PR may be sufficient to justify tandem over traditional SJ modules in some niche applications, but for large-scale adoption, technical performance alone is not enough. Instead, LCOE becomes the deciding factor. At this stage, accurate prediction of absolute manufacturing cost for tandem modules is difficult due to uncertainties such as the actual equipment involved, process and fabrication steps, and manufacturing yield. Therefore, we show a comparative study with a high-efficiency industrial SJ PERC Si module as a benchmark. We illustrate the competitiveness of tandems by calculating their allowed fabrication cost increase in relative percentage of Si module manufacturing cost to reach the same LCOE as SJ Si, with other system-level cost components held constant. This allowed increase is referred to here as "cost premium.". The cost premium represents an upper limit that any added cost of top and bottom cells as well as tandem module integration must fall below to stay competitive with SJ Si, which will likely maintain its dominant role in years to come.

Figure 8 shows the calculated worldwide cost premium of the 34.2% efficient 4T GaAs-Si tandem module. In this exercise, we take into consideration the $Y_f$ (which is determined by insolation level and the implied PR), the module fabrication costs, and various other cost factors taken from the residential PV scenario using country-specific cost information (see Experimental Procedures). The color saturation in Figure 8 represents the allowed cost premium of 4T GaAs-Si tandem. The global minimum is ~150%, but we only show values >180%, which marks the 5th percentile. The green color indicates that the cost premium of all other tandem architectures surpasses this level, whereas the blue color indicates that only the cost premium of 4T does (and in most cases, 3T and VM also do). While the green regions indicate good opportunity for all of the tandem architectures, the blue regions suggest that 3T, 4T, and VM are more likely to become competitive. In many places, all of the tandems allow doubling of the current level of Si module fabrication cost (100% cost premium). For 4T and 3T-VM, the tripling of manufacturing cost is allowed in most places. This is not so in cold climates, high-altitude mountains, regions with low insolation, and some parts of the tropics. In high-value markets with high insolation, the allowed cost premium can even reach 500%. The most promising regions for

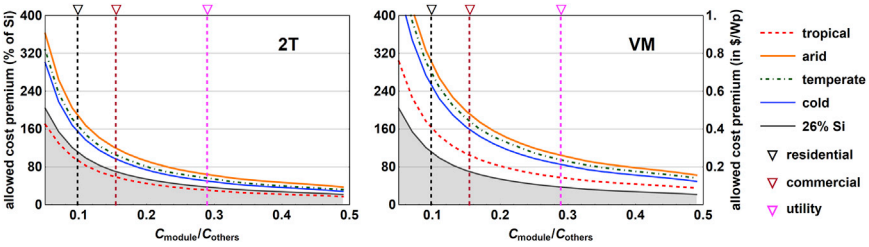


**Figure 9. Cost Premium Sensitivities**

The 90th percentile value of allowed cost premium for 2T and VM GaAs-Si tandems in each climate zone as a function of decreasing $C_{others}$, inclusive of life-cycle costs discounted to present values. Three cost scenarios are indicated in the figure: residential, commercial, and utility. Values indicated at the x axis represent the US case only, with cost ratios of 0.1, 0.15, and 0.29, respectively for the three scenarios. The same x axis positions would have different values for other countries. The situation for AM and 4T configuration is similar to that of 2T and VM, respectively. The allowed premium for a 26% efficient SJ Si module is also shown in gray.

tandems include Australia, the southern United States, and the Middle East. Canada, Japan, New Zealand, and western Europe also allow high cost premiums due to the high installation and maintenance costs. This indicates that there is some room for tandems to compete with SJ Si in high-value residential markets, corroborating the conclusions of previous studies.[5,24]

Commercial and utility-scale deployment has a very different cost structure from residential systems. Cognizant that BOS and soft costs in the residential scenario are relatively high, we also show how the allowable cost premium depends on these costs. This serves as a sensitivity analysis on the assumed costs. Figure 9 shows the allowed cost premium for 2T and VM GaAs-Si as a function of BOS plus other remaining costs ($C_{others}$) in the best markets (90th percentile) of various climates, while keeping the PERC Si module cost ($C_{module}$) constant at \$0.25/$W_p$. The situation is different for different climate zones, as seen from the spread of the different color lines. In general, the allowed cost premium is highest in arid climates. In the tropics, the allowed cost premium is lowest due to the generally low $C_{others}$ in tropical countries. This is the case even for VM tandem (and similarly for 3T and 4T), which demonstrates superior technical performance in these regions. The allowed cost premium declines rapidly as $C_{others}$ decreases (thus higher $C_{module}/C_{others}$). In the utility scenario (violet vertical dashed line), the allowed cost premium falls below 100%, making it much harder for tandems to compete. This agrees with conclusions derived from more detailed techno-economic analyses in previous studies.[4,5,24] However, a more than doubling of the cost (allowed cost premium >100%) is still supported for commercial applications (dark red vertical dashed line). Figure 9 also shows the average allowed cost premium for a 26% efficient SJ Si. For 2T GaAs-Si, the additional margin for allowed cost increase (space above the gray area) is much smaller than that of VM.

## DISCUSSION

In this work, we investigated the worldwide outdoor performance potential of five tandem module architectures with a variety of material combinations, including GaAs on Si and perovskite on Si, and the implications on cost competitiveness. In particular, we establish an evaluation framework for globally assessing different module configurations from the new angle of outdoor PR, on top of efficiency and absolute energy yield.

In most parts of the world, the high efficiency of tandems is proportionally translated into superior yield. In absolute terms, we find global median yield improvements compared to conventional SJ Si PV modules (median yield 268 kWh/$m^2$) of 112 kWh/$m^2$ (+40% relative) and 160 kWh/$m^2$ (+60% relative) for the current record-level perovskite-on-Si and GaAs-on-Si tandems, respectively.

Most notably, we observe that the choice of the best tandem architecture depends on the characteristic of the sub-cells and operating conditions: if a tandem module with other architectures could be made at the same STC efficiency as a 4T module (despite imperfect current or voltage matching), then it is possible to outperform the 4T module in the field. In general, our calculation indicates the voltage-matching architectures (3T and mechanically VM tandem) to be promising candidates for achieving superior outdoor performance if they can achieve good STC efficiency. With the same installed capacity, 3T and VM tandem modules deliver nearly equal (>98%) or even more than the power that is achievable by 4T tandems, which is commonly regarded as the ideal tandem in terms of yield. The PR of the tandems with voltage-matching architectures is superior to that of Si modules in hot and sunny regions, including the vast majority of Africa, South Asia and Southeast Asia, the Middle East, Central and South America, and Australia. Current matching tandems (2T and AM) generally show significantly lower PRs in all but the cold climates, only reaching 94%–98% of the 4T yield. Hence, the customization of tandem design is desirable, especially in the tropics, where approximately half of the spectral losses can be recovered.[27] In temperate and arid climates, all of the tandem architectures reach PR levels that are similar (>97%) to conventional Si modules.

In addition, we investigate the boundary conditions for tandem modules to be economically successful. We find that even for the same module configuration, economic competitiveness differs significantly in different climates and geolocations. Compared to mainstream Si technology, tandems have the greatest opportunities in areas that have a high insolation and high BOS costs. Using residential market conditions as a baseline, we find that doubling, for tandems in general, or even a five times increase in manufacturing cost, for 3T, 4T, and VM tandems in certain regions compared to PERC Si technology ($0.25/$W_p$) would still result in a lower LCOE. 3T, 4T, and VM tandems would support the doubling of manufacturing costs in commercial and even utility-scale applications under the most optimistic scenarios. Therefore, tandem technology is potentially promising for future residential applications, and may even become viable for large-scale installations, especially in high-value markets from arid climates.

To move forward, the availability of top cells that combine low fabrication cost and high efficiency remains the key to making tandems viable. Perovskite technology appears to be a very promising candidate. Literature estimates indicate that cost premiums for integrating perovskite onto Si monolithically would be <20%.[44] Module-level integration would be more costly, but the additional cost is arguably still lower than making standalone perovskite modules, which are projected by several cost analyses to be comparable to or cheaper than Si modules.[5,24,45–47] However, module integration would require innovation on top cell structure and fabrication processes to enable effective encapsulation of top semi-transparent half-module with the Si bottom half. III-V-on-Si technology is presently too expensive due to the high costs associated with the III-V deposition process, but it could become an option if progress in large-scale high-throughput epitaxial growth (e.g., rapid growth rate metalorganic vapor phase epitaxy [MOVPE][48,49]) proves successful. Together with other measures, it may be possible to achieve a III-V solar cell

fabrication cost below $0.5/W$_{DC}$[50], making a cost premium of <200% possible. However, significant research is still required to realize high efficiency with these low-cost pathways. Another force that can tip the balance is the inclusion of energy storage to the system in the future, which further reduces the proportion of module cost in the total cost structure, and hence favors high-performance tandem modules. At present, we believe that tandem modules should be optimized to arid conditions instead of STCs when making the initial entry into the market.

## EXPERIMENTAL PROCEDURES

### Device Modeling

Tandem device output is modeled using a coupled optoelectronic model taking into consideration photon recycling and LC. Optical absorption and current generation under arbitrary incoming spectra are calculated primarily with experimentally measured cell/sub-cell EQE from the literature, except for 2T GaAs on Si, for which no reliable measurement is available and in which the optical simulation coupling transfer matrix method and ray tracing (a method developed by Liu et al.[37]) are used. With the calculated photogeneration current density in the SJ solar cell or each sub-cell in a tandem, the individual IV curves are simulated, assuming superior electrical properties found in record cells. III-V and Si cells are modeled with the widely used two-diode model. However, the two-diode model may not account for important physical effects such as a voltage-dependent carrier collection in p-i-n or heterojunction types of devices.[51,52] Therefore, a physics-based model by Sun et al.[36] is used instead for modeling the metal halide perovskite cells to give better results under a diverse range of operating conditions.[53] However, shunt resistance is not included in the perovskite model, which gives it exceptional low-light performance and high PR. This is likely not the case when scaling up. In some high-efficiency tandems (e.g., III-V-on-Si), photon recycling and LC are important phenomena that should be accounted for to accurately describe their behavior.[54,55] In this process, electroluminescence and photoluminescence from high bandgap sub-cells not only enhance their own electrical property via photon recycling but can also be optically coupled to lower bandgap sub-cells below. This can alter the tandem behavior significantly under different illumination conditions.[43] Hence, we adopted the optoelectronic model from Geisz et al.[35] in the present study to reflect the impact of photon recycling and coupling efficiency on the yield of various tandem architectures. This model takes into account the internal photon recycling effect and also adjusts the photogeneration current of lower bandgap sub-cells based on the operating point of the high bandgap cell above them. The IV of each sub-cell is then combined into a tandem IV based on the given tandem architecture according to a simple circuit model (see Supplemental Experimental Procedures).

In addition, we have considered the effect of operating temperature. In the two-diode model and the physics-based model, we treated temperature dependence by taking into account the theoretical temperature dependence of bandgap ($E_g$), diode saturation currents ($J_0$), and the short-circuit current ($J_{sc}$) according to established models in the literature.[56–61] The operating temperature given the ambient temperature, irradiance level, and device efficiency is calculated using an empirical model from the energy balance assumption.[62,63]

Overall, this simulation framework is among the most sophisticated in energy yield studies, which provides a theoretical case study. However, readers should be aware of its limitations in representing arbitrary real devices accurately: (1) EQE dependence on temperature and other effects such as angle are not considered, other

than the linear dependence of $J_{sc}$ on temperature; (2) theoretical temperature dependence may be slightly different in real devices with different cell architectures and fabrication processes; (3) accurate analytical models for different types of perovskite solar cells are not yet fully established; (4) resistive effects are not investigated, especially shunt resistance, which has a significant effect on low-light performance; (5) degradation is not modeled—only a fixed degradation rate is assumed during LCOE calculations. As a result, the exact outdoor performance of an actual device needs to be recalculated using calibrated models. More details and parameters assumed for the models can be found in Figure S1 and Tables S1–S3.

### Energy Yield and Field Performance Calculation

Our global energy yield calculation routine is adopted and modified from the method developed by Peters et al.[34] Daily average values of operating environment parameters, including solar irradiance, ambient temperature, humidity, ground reflectance, and aerosol are taken from NASA's various satellite instruments in the Earth Observing System (Database: CERES SSF1deg).[64–66] We have compared and validated the satellite readings against ground weather stations (Table S4; Supplemental Experimental Procedures). The solar spectrum is calculated with the simple model of the atmospheric radiative transfer of sunshine (SMARTS).[67] Using the device modeling outlined above, we calculate the yield for each day and each location above sea level, with a spatial resolution of 1° × 1°. We considered losses (or gains) due to irradiance levels, varying spectrum, and module temperature. This methodology has achieved a good match between predicted field performance in terms of PR and experimentally measured results for Si and cadmium telluride (CdTe) technologies in Singapore and Perrysburg, Ohio.[34] In the present work, we have made further refinements by adjusting the daily average irradiance values to reflect the most representative condition during the daytime. In addition, we have used in-plane irradiance tilted at latitude angle (converted from horizontal irradiance) to obtain the absolute yield.

In addition, we describe the worldwide outdoor field performance by both energy yield and implied PR.[27] This PR characterizes how the device performs in the field relative to how it performs under STCs, which is an important metric for PV system designers in real-world applications. It is a normalized measure of outdoor performance that facilitates comparison between different devices. In general, PR tends to show less sensitivity toward the assumed device parameters and is thus more generalizable than energy yield alone. Furthermore, in actual project developments, financial performance is of the utmost importance, which involves using PR to estimate the actual performance from nameplate performance. Module field performance and other related losses will be factored in when sourcing equipment (e.g., choosing technologies). Discussions on the energy yield potential at the radiative limit are abundant in the literature[12,28] and will not be treated further in this article. PR here only reflects losses from the inherent behavior of the devices (therefore the name "implied PR") and does not account for losses from other system components such as cables and inverters. This distinction is important, as it marks the difference from the term "performance ratio" as it is used in PV system measurements.[68,69] Nevertheless, it is a convenient measure that is directly interpretable by system researchers. Long-term changes in PR due to degradation are also neglected.

We have used data from 2015 to perform the calculation. It should be noted that insolation and operating conditions fluctuate from year to year. However, in previous work, we found that calculated PR shows a small sensitivity toward year-to-year variation,[70] and therefore is a robust measure that can be generalized. The annual insolation, however, varies by ~10%.[71] Another factor that influences the calculated results is the assumed value of LC. Here, we briefly assessed its impact and found that the maximum difference in calculated PR between the cases with no LC and with full coupling efficiency is ~0.03 for 2T GaAs on Si tandem (Figures S9 and S10; Note S4).

## LCOE Calculations

LCOE is a well-known figure of merit to compare the economics of electricity production. It is calculated by dividing the total lifetime cost by the total lifetime electricity production. Here, we use the general equation below to compute LCOE:

$$LCOE = \frac{C_{module} \times P + BOS_{area} \times A + BOS_{power} \times P + C_{project} + C_{others} + \sum_{i=0}^{N} \frac{O\&M}{(1+r)^i}}{\sum_{i=0}^{N} \frac{Y_f \times (1-d)^i}{(1+r)^i}} \quad (1)$$

where $C_{module}$ is the module cost in \$/$W_p$, $BOS$ is the balance of system cost broken down into components that scale with the system area ($A$) and system capacity ($P$), $C_{project}$ represents various project-related costs such as taxes and overhead, $C_{others}$ denotes other costs such as financial costs and replacement costs, $O\ \&\ M$ is the annual cost of operation and maintenance, $N$ is the system lifetime, $Y_f$ is the final energy yield of the first year, $d$ is the degradation rate, and $r$ is the nominal discount rate. Here, we consider only inverter replacement cost in the 15$^{th}$ year as $C_{others}$, and no financial costs are included.

As tandem technology will most likely make its way initially into real-world applications in small-scale residential markets, we calculate the global costs for a residential scenario. The 2018 cost data from the United States is taken as a baseline.[72] For other countries, the costs are scaled by comparing the country-specific utility installation cost, maintenance cost, and discount rate (based on the Solar Energy Research Institute of Singapore [SERIS] curation of financial cost data[73]) to those of the United States. Here, we make a simplifying assumption that the same scaling applies to commercial and residential scenarios. The ex-factory gate price of a benchmark decent efficiency PERC Si module ($C_{PERC\ Si}$) is assumed to be the same at \$0.25/$W_p$ for all cases and all countries. For a residential scenario, markup due to supply chain cost exists, which was added to BOS costs that scale with power. In this way, we can separate module fabrication cost from all of the other costs related to the system and project. The tandem module fabrication cost is represented by this benchmark module price multiplied by a factor (1 + $x$), where $x$ is the cost premium compared to making a conventional Si module. Given the calculated yield for Si ($Y_{f\_PERC\ Si}$) and for the various tandems ($Y_{f\_tandem}$), we then solve for each location the cost premium $x$ that makes LCOE of Si and tandem modules equal (Equation 2):

$$LCOE\left(C_{PERC\ Si}, BOS_{PERC\ Si}, Y_{f\_PERC\ Si}, \ldots\right) = LCOE\left(C_{PERC\ Si} \times (1+x), BOS_{tandem}, Y_{f\_tandem}, \ldots\right) \quad (2)$$

It is known that the competitiveness of tandem technology depends significantly on the cost structure (i.e., the proportion of BOS and other costs).[4,5,24] In utility-scale systems, this proportion would be much lower. Therefore, we also sweep the value of BOS plus other costs to shed light on other types of

deployment that have different cost structures. More details about the cost figures and assumptions in the calculation are presented in Table S6 and Figures S11–S13.

## DATA AND CODE AVAILABILITY

The codes used for performing the simulation are available on GitHub (https://github.com/Haohui88/analytical-solar-cell-and-module). All of the data are available from the corresponding author upon reasonable request.

## SUPPLEMENTAL INFORMATION

Supplemental Information can be found online at https://doi.org/10.1016/j.xcrp.2020.100037.

## ACKNOWLEDGMENTS

This work was supported by SERIS and the Singapore-MIT Alliance for Research and Technology (SMART). SERIS is supported by the National University of Singapore (NUS) and Singapore's National Research Foundation Singapore (NRF) through the Singapore Economic Development Board (EDB). We would also like to acknowledge NASA as the source of the satellite data.

## AUTHOR CONTRIBUTIONS

H.L. developed device models for tandem modules, with optical inputs contributed by Z.L. I.M.P. developed the global energy yield calculation methodology, with refinements from H.L. and C.D.R.-G. C.D.R.-G. validated the satellite data with selected ground weather stations. H.L. performed the calculation, analysis, and data visualization, with valuable feedback from I.M.P., C.D.R.-G., Z.L., T.B., and T.R. H.L., I.M.P., Z.L., T.B., and T.R. were involved in the initial conceptualization of the project. The manuscript was written mainly by H.L. and edited by all of the co-authors. All of the authors reviewed and approved the manuscript.

## DECLARATION OF INTERESTS

The authors declare no competing interests.

Received: August 29, 2019
Revised: February 10, 2020
Accepted: February 19, 2020
Published: April 8, 2020

## REFERENCES

1. Green, M.A., Dunlop, E.D., Levi, D.H., Hohl-Ebinger, J., Yoshita, M., and Ho-Baillie, A.W.Y. (2019). Solar cell efficiency tables (version 54). Prog. Photovolt. *27*, 565–575.

2. Kayes, B.M., Hui, N., Twist, R., Spruytte, S.G., Reinhardt, F., Kizilyalli, I.C., and Higashi, G.S. (2011). 27.6% conversion efficiency, a new record for single-junction solar cells under 1 sun illumination. https://ieeexplore.ieee.org/document/6185831.

3. Yoshikawa, K., Kawasaki, H., Yoshida, W., Irie, T., Konishi, K., Nakano, K., Uto, T., Adachi, D., Kanematsu, M., Uzu, H., and Yamamoto, K. (2017). Silicon heterojunction solar cell with interdigitated back contacts for a photoconversion efficiency over 26%. Nat. Energy *2*, 17032.

4. Peters, I.M., Sofia, S., Mailoa, J., and Buonassisi, T. (2016). Techno-economic analysis of tandem photovoltaic systems. RSC Adv. *6*, 66911–66923.

5. Yu, Z.J., Carpenter, J.V., and Holman, Z.C. (2018). Techno-economic viability of silicon-based tandem photovoltaic modules in the United States. Nat. Energy *3*, 747–753.

6. Essig, S., Allebé, C., Remo, T., Geisz, J.F., Steiner, M.A., Horowitz, K., Barraud, L., Ward, J.S., Schnabel, M., Descoeudres, A., et al. (2017). Raising the one-sun conversion efficiency of III–V/Si solar cells to 32.8% for two junctions and 35.9% for three junctions. Nat. Energy *6*, 17144.

7. Cariou, R., Benick, J., Feldmann, F., Höhn, O., Hauser, H., Beutel, P., Razek, N., Wimplinger, M., Bläsi, B., Lackner, D., et al. (2018). III–V-on-silicon solar cells reaching 33% photoconversion efficiency in two-terminal configuration. Nat. Energy *3*, 326–333.

8. Jaysankar, M., Qiu, W., Eerden, M.V., Aernouts, T., Gehlhaar, R., Debucquoy, M., Paetzold, U.W., and Poortmans, J. (2017). Four-Terminal Perovskite/Silicon Multijunction Solar Modules. Adv. Energy Mater. *7*, 1602807.

9. Sahli, F., Werner, J., Kamino, B.A., Bräuninger, M., Monnard, R., Paviet-Salomon, B., Barraud, L., Ding, L., Diaz Leon, J.J., Sacchetto, D., et al.

(2018). Fully textured monolithic perovskite/silicon tandem solar cells with 25.2% power conversion efficiency. Nat. Mater. *17*, 820–826.

10. Yang, J., Peng, Z., Cheong, D., and Kleiman, R.N. (2012). III-V on Silicon Multi-Junction Solar Cell with 25% 1-Sun Efficiency via Direct Metal Interconnect and Areal Current Matching. https://doi.org/10.4229/27thEUPVSEC2012-1BO.12.6.

11. MacAlpine, S., Bobela, D.C., Kurtz, S., Lumb, M.P., Schmieder, K.J., Moore, J.E., Walters, R.J., and Alberi, K. (2017). Simulated potential for enhanced performance of mechanically stacked hybrid III–V/Si tandem photovoltaic modules using DC–DC converters. J. Photonics Energy *7*, 042501.

12. Futscher, M.H., and Ehrler, B. (2016). Efficiency Limit of Perovskite/Si Tandem Solar Cells. ACS Energy Lett. *1*, 863–868.

13. Gee, J.M. (1988). A comparison of different module configurations for multi-band-gap solar cells. Sol. Cells *24*, 147–155.

14. Warren, E.L., Deceglie, M.G., Rienacker, M., Peibst, R., Tamboli, A.C., and Stradins, P. (2018). Maximizing tandem solar cell power extraction using a three-terminal design. Sustain. Energy Fuels *2*, 1141–1147.

15. Rienäcker, M., Warren, E.L., Schnabel, M., Schulte-Huxel, H., Niepelt, R., Brendel, R., Stradins, P., Tamboli, A.C., and Peibst, R. (2019). Back-contacted bottom cells with three terminals: maximizing power extraction from current-mismatched tandem cells. Prog. Photovolt. *27*, 410–423.

16. Schulte-Huxel, H., Friedman, D.J., and Tamboli, A.C. (2018). String-Level Modeling of Two, Three, and Four Terminal Si-Based Tandem Modules. IEEE J. Photovolt. *8*, 1370–1375.

17. Soga, T., Yang, M., Jimbo, T., and Umeno, M. (1996). High-Efficiency Monolithic Three-Terminal GaAs/Si Tandem Solar Cells Fabricated by Metalorganic Chemical Vapor Deposition. Jpn. J. Appl. Phys. *35*, 1401.

18. Steiner, M.A., Wanlass, M.W., Carapella, J.J., Duda, A., Ward, J.S., Moriarty, T.E., and Emery, K.A. (2009). A monolithic three-terminal GaInAsP/GaInAs tandem solar cell. Prog. Photovolt. *17*, 587–593.

19. Emziane, M., and Nicholas, R.J. (2007). Double-junction three-terminal photovoltaic devices: a modeling approach. J. Appl. Physiol. *102*, 074508.

20. Kurtz, S.R., Faine, P., and Olson, J.M. (1990). Modeling of two-junction, series-connected tandem solar cells using top-cell thickness as an adjustable parameter. J. Appl. Physiol. *68*, 1890–1895.

21. Martí, A., and Araújo, G.L. (1996). Limiting efficiencies for photovoltaic energy conversion in multigap systems. Sol. Energy Mater. Sol. Cells *43*, 203–222.

22. Brown, A.S., and Green, M.A. (2002). Detailed balance limit for the series constrained two terminal tandem solar cell. Physica E Low Dimens. Syst. Nanostruct. *14*, 96–100.

23. Ryyan Khan, M., and Alam, M.A. (2015). Thermodynamic limit of bifacial double-junction tandem solar cells. Appl. Phys. Lett. *107*, 223502.

24. Sofia, S.E., Mailoa, J.P., Weiss, D.N., Stanbery, B.J., Buonassisi, T., and Peters, I.M. (2018). Economic viability of thin-film tandem solar modules in the United States. Nat. Energy *3*, 387–394.

25. Faine, P., Kurtz, S.R., Riordan, C., and Olson, J.M. (1991). The influence of spectral solar irradiance variations on the performance of selected single-junction and multijunction solar cells. Sol. Cells *31*, 259–278.

26. Liu, H., Ren, Z., Liu, Z., Aberle, A.G., Buonassisi, T., and Peters, I.M. (2015). The realistic energy yield potential of GaAs-on-Si tandem solar cells: a theoretical case study. Opt. Express *23*, A382–A390.

27. Liu, H., Ren, Z., Liu, Z., Aberle, A.G., Buonassisi, T., and Peters, I.M. (2017). Predicting the outdoor performance of flat-plate III–V/Si tandem solar cells. Sol. Energy *149*, 77–84.

28. Futscher, M.H., and Ehrler, B. (2017). Modeling the Performance Limitations and Prospects of Perovskite/Si Tandem Solar Cells under Realistic Operating Conditions. ACS Energy Lett. *2*, 2089–2095.

29. Horantner, M.T., and Snaith, H.J. (2017). Predicting and optimising the energy yield of perovskite-on-silicon tandem solar cells under real world conditions. Energy Environ. Sci. *10*, 1983–1993.

30. Duck, B.C., Dunbar, R.B., Lee, O., Anderson, K.F., Jones, T.W., Wilson, G.J., and Fell, C.J. (2016). Energy yield potential of perovskite-silicon tandem devices. In 2016 IEEE 43rd Photovoltaic Specialists Conference (PVSC), Portland, OR, pp. 1624–1629.

31. Dupré, O., Niesen, B., De Wolf, S., and Ballif, C. (2018). Field Performance versus Standard Test Condition Efficiency of Tandem Solar Cells and the Singular Case of Perovskites/Silicon Devices. J. Phys. Chem. Lett. *9*, 446–458.

32. Schulte-Huxel, H., Silverman, T.J., Deceglie, M.G., Friedman, D.J., and Tamboli, A.C. (2018). Energy Yield Analysis of Multiterminal Si-Based Tandem Solar Cells. IEEE J. Photovolt. *8*, 1376–1383.

33. Schmager, R., Langenhorst, M., Lehr, J., Lemmer, U., Richards, B.S., and Paetzold, U.W. (2019). Methodology of energy yield modelling of perovskite-based multi-junction photovoltaics. Opt. Express *27*, A507–A523.

34. Peters, I.M., Liu, H., Reindl, T., and Buonassisi, T. (2018). Global Prediction of Photovoltaic Field Performance Differences Using Open-Source Satellite Data. Joule *2*, 307–322.

35. Geisz, J.F., Steiner, M.A., García, I., France, R.M., McMahon, W.E., Osterwald, C.R., and Friedman, D.J. (2015). Generalized Optoelectronic Model of Series-Connected Multijunction Solar Cells. IEEE J. Photovolt. *5*, 1827–1839.

36. Sun, X., Asadpour, R., Nie, W., Mohite, A.D., and Alam, M.A. (2015). A Physics-Based Analytical Model for Perovskite Solar Cells. IEEE J. Photovolt. *5*, 1389–1394.

37. Liu, Z., Ren, Z., Liu, H., Sahraei, N., Lin, F., Stangl, R., Aberle, A.G., Buonassisi, T., and Peters, I.M. (2017). A modeling framework for optimizing current density in four-terminal tandem solar cells: a case study on GaAs/Si tandem. Sol. Energy Mater. Sol. Cells *170*, 167–177.

38. Werner, J., Barraud, L., Walter, A., Bräuninger, M., Sahli, F., Sacchetto, D., Tétreault, N., Paviet-Salomon, B., Moon, S.-J., Allebé, C., et al. (2016). Efficient Near-Infrared-Transparent Perovskite Solar Cells Enabling Direct Comparison of 4-Terminal and Monolithic Perovskite/Silicon Tandem Cells. ACS Energy Lett. *1*, 474–480.

39. Fell, A., McIntosh, K.R., Altermatt, P.P., Janssen, G.J.M., Stangl, R., Ho-Baillie, A., Steinkemper, H., Greulich, J., Muller, M., Min, B., et al. (2015). Input Parameters for the Simulation of Silicon Solar Cells in 2014. IEEE J. Photovolt. *5*, 1250–1263.

40. Yang, W.S., Park, B.-W., Jung, E.H., Jeon, N.J., Kim, Y.C., Lee, D.U., Shin, S.S., Seo, J., Kim, E.K., Noh, J.H., and Seok, S.I. (2017). Iodide management in formamidinium-lead-halide-based perovskite layers for efficient solar cells. Science *356*, 1376–1379.

41. Geisz, J.F., Steiner, M.A., García, I., Kurtz, S.R., and Friedman, D.J. (2013). Enhanced external radiative efficiency for 20.8% efficient single-junction GaInP solar cells. Appl. Phys. Lett. *103*, 041118.

42. Liu, H., Aberle, A.G., Buonassisi, T., and Peters, I.M. (2016). On the methodology of energy yield assessment for one-Sun tandem solar cells. Sol. Energy *135*, 598–604.

43. Ren, Z., Mailoa, J.P., Liu, Z., Liu, H., Siah, S.C., Buonassisi, T., and Peters, I.M. (2015). Numerical Analysis of Radiative Recombination and Reabsorption in GaAs/Si Tandem. IEEE J. Photovoltaics *5*, 1079–1086.

44. Leijtens, T., Bush, K.A., Prasanna, R., and McGehee, M.D. (2018). Opportunities and challenges for tandem solar cells using metal halide perovskite semiconductors. Nat. Energy *3*, 828–838.

45. Cai, M., Wu, Y., Chen, H., Yang, X., Qiang, Y., and Han, L. (2016). Cost-Performance Analysis of Perovskite Solar Modules. Adv. Sci. (Weinh.) *4*, 1600269.

46. Chang, N.L., Yi Ho-Baillie, A.W., Basore, P.A., Young, T.L., Evans, R., and Egan, R.J. (2017). A manufacturing cost estimation method with uncertainty analysis and its application to perovskite on glass photovoltaic modules. Prog. Photovolt. *25*, 390–405.

47. Song, Z., McElvany, C.L., Phillips, A.B., Celik, I., Krantz, P.W., Watthage, S.C., Liyanage, G.K., Apul, D., and Heben, M.J. (2017). A technoeconomic analysis of perovskite solar module manufacturing with low-cost materials and techniques. Energy Environ. Sci. *10*, 1297–1305.

48. Lang, R., Schön, J., Dimroth, F., and Lackner, D. (2018). Optimization of GaAs Solar Cell Performance and Growth Efficiency at MOVPE Growth Rates of 100 µm/h. IEEE J. Photovolt. *8*, 1596–1600.

49. Ubukata, A., Sodabanlu, H., Watanabe, K., Koseki, S., Yano, Y., Tabuchi, T., Sugaya, T., Matsumoto, K., Nakano, Y., and Sugiyama, M. (2018). Accelerated GaAs growth through

MOVPE for low-cost PV applications. J. Cryst. Growth *489*, 63–67.

50. Horowitz, K.A., Remo, T.W., Smith, B., and Ptak, A.J. (2018). A Techno-Economic Analysis and Cost Reduction Roadmap for III-V Solar Cells (National Renewable Energy Laboratory).

51. Boyd, M.T., Klein, S.A., Reindl, D.T., and Dougherty, B.P. (2011). Evaluation and Validation of Equivalent Circuit Photovoltaic Solar Cell Performance Models. J. Sol. Energy Eng. *133*, 021005–021018.

52. Sun, X., Silverman, T., Garris, R., Deline, C., and Alam, M.A. (2016). An Illumination- and Temperature-Dependent Analytical Model for Copper Indium Gallium Diselenide (CIGS) Solar Cells. IEEE J. Photovolt. *6*, 1298–1307.

53. Silvestre, S., Mas-Marzá, E., Puigdollers, J., Fabregat-Santiago, F., and Alfonso, V.G. (2017). Comparison of Simulation Models for Perovskite Solar Cells. In 33rd European Photovoltaic Solar Energy Conference and Exhibition. https://www.researchgate.net/publication/322152898_Comparison_of_simulation_models_for_Perovskite_solar_cells.

54. Miller, O.D., Yablonovitch, E., and Kurtz, S.R. (2012). Strong Internal and External Luminescence as Solar Cells Approach the Shockley-Queisser Limit. IEEE J. Photovolt. *2*, 303–311.

55. Friedman, D.J., Geisz, J.F., and Steiner, M.A. (2014). Effect of Luminescent Coupling on the Optimal Design of Multijunction Solar Cells. IEEE J. Photovolt. *4*, 986–990.

56. Singh, P., and Ravindra, N.M. (2012). Temperature dependence of solar cell performance—an analysis. Sol. Energy Mater. Sol. Cells *101*, 36–45.

57. Dupré, O., Vaillon, R., and Green, M.A. (2015). Physics of the temperature coefficients of solar cells. Sol. Energy Mater. Sol. Cells *140*, 92–100.

58. Green, M.A. (2003). General temperature dependence of solar cell performance and implications for device modelling. Prog. Photovolt. *11*, 333–340.

59. Varshni, Y.P. (1967). Temperature dependence of the energy gap in semiconductors. Physica *34*, 149–154.

60. Foley, B.J., Marlowe, D.L., Sun, K., Saidi, W.A., Scudiero, L., Gupta, M.C., and Choi, J.J. (2015). Temperature dependent energy levels of methylammonium lead iodide perovskite. Appl. Phys. Lett. *106*, 243904.

61. Milot, R.L., Eperon, G.E., Snaith, H.J., Johnston, M.B., and Herz, L.M. (2015). Temperature-Dependent Charge-Carrier Dynamics in CH3NH3PbI3 Perovskite Thin Films. Adv. Funct. Mater. *25*, 6218–6227.

62. Skoplaki, E., and Palyvos, J.A. (2009). Operating temperature of photovoltaic modules: a survey of pertinent correlations. Renew. Energy *34*, 23–29.

63. Faiman, D. (2008). Assessing the outdoor operating temperature of photovoltaic modules. Prog. Photovolt. *16*, 307–315.

64. National Aeronautics and Space Administration.. Clouds and Earth's Radiant Energy System (CERES). https://ceres.larc.nasa.gov/.

65. National Aeronautics and Space Administration.. Atmospheric Infrared Sounder (AIRS). https://airs.jpl.nasa.gov/.

66. National Aeronautics and Space Administration.. Moderate Resolution Imaging Spectroradiometer (MODros. Inf. Serv.). https://modis.gsfc.nasa.gov/.

67. Gueymard, C. (1995). SMARTS2: A Simple Model of the Atmospheric Radiative Transfer of Sunshine: Algorithms and Performance Assessment. Report FSEC-PF-270-95 (Florida Solar Energy Center).

68. Reich, N.H., Mueller, B., Armbruster, A., van Sark, W.G.J.H.M., Kiefer, K., and Reise, C. (2012). Performance ratio revisited: is PR > 90% realistic? Prog. Photovolt. *20*, 717–726.

69. International Electrotechnical Commission (1998). Photovoltaic System Performance Monitoring—Guidelines for Measurement, Data Exchange and Analysis. BS EN 61724/IEC 61724. file:///C:/Users/Owner/Downloads/IEC61724%20PV%20monitoring.pdf.

70. Liu, H. (2016). Energy Yield Calculation for Silicon Based Tandem Solar Cells. Ph.D thesis (National University of Singapore).

71. Ineichen, P. (2011). Global irradiation: average and typical year, and year to year annual variability. In University of Geneva, Institute for Environmental Science Solar World Congress 2011. https://pdfs.semanticscholar.org/4594/7fabc756cc3fcb7e0f2f48d762c9d96bdf5b.pdf.

72. Fu, F., Feldman, D., and Margolis, R. (2018). U.S. Solar Photovoltaic System Cost Benchmark: Q1: 2018NREL/TP-6A20-72399 (National Renewable Energy Laboratory).

73. Rodríguez-Gallegos, C.D., Bieri, M., Gandhi, O., Singh, J.P., Reindl, T., and Panda, S.K. (2018). Monofacial vs bifacial Si-based PV modules: which one is more cost-effective. Sol. Energy *176*, 412–438.